1

On the Use of Photothermal Techniques as a Tool to Characterize Ceramic-Metal Materials

F. A. L. Machado, M. Filgueira, R. T. Faria Jr. and H. Vargas
Universidade Estadual do Norte Fluminense Darcy Ribeiro, Campos dos Goytacazes-RJ Brazil

1. Introduction

Since the discovery of the photoacoustic effect by Bell in 1881 (Bell, 1880), the so-called photoacoustic techniques have experienced great expansion. Since 1980, approximately, they have been used in a wide range of scientific areas. The photoacoustic and related photothermal techniques have proved to be a valuable tool to thermal characterization of solids, liquids and gases (Vargas & Miranda, 2003). This is one of the non-destructive laser-induced photothermal techniques that are based on the detection of periodic thermal waves generated due to a non-radiative de-excitation in the sample, which is illuminated by a chopped or pulsed optical excitation. In this chapter, thermal and structural characteristics of hardmetal (WC-10%wt Co) alloys were examined.

Hardmetal is a composite material (ceramic-metal) comprised by hard tungsten carbide – WC grains or particles, embedded into a tough binder – normally cobalt - Co (Allibert, 2001). Co percolates the WC particles, forming the WC-Co structure – the most common hardmetal alloy.

The hardmetal's formation occurs through the liquid phase sintering of the as compacted WC and Co powders, at temperatures roughly about 1400ºC, in which Co spreads around WC grains and particles, enabling homogeneity, density, hardness and other desired properties.

Both phases can be modified, aiming at achieving the final desired properties (Upadhyaya, 2001). As an example, the binder phase amount is linked to the hardmetal properties, that is, as large is the Co amount, as lower is the hardness, but the fracture toughness is substantially improved.

Hardmetals present high hardness, good wear resistance, and considerable fracture toughness, allied with interesting thermal properties. These materials have been widely used in industry, due to the excellent combination among wear, impact, compressive resistance, high elastic modulus, corrosion and thermal shock resistance (Allibert, 2001; Fang *et al*., 2009). Therefore, due to the high stability and excellent mechanical properties, their main applications includes the cutting tools in general, oil and gas well drills, forming parts – such as wire drawings tools, high energy milling components, among others (Gille *et al* ., 2002).

Thermal characterization plays an important role to qualify hardmetals, rare are the literatures with the purpose of analyzing these properties (Faria Jr. et al., 2005, Kny & Neumann, 1985). This study intends to discuss the thermal behavior in six diversified WC-

10%wtCo samples (table 1), which are sintered in a not-conventional route metallurgic powder named high pressure-high temperature (HPHT), normally used to produce synthetic diamonds. For more details of HPHT see references (Faria Jr. et al., 2005, Osipov, et al., 2003).

2. Experimental

2.1 Samples

Figure 1 shows the route employed to process the hardmetal WC-10%wtCo. Commercial powders of WC and Co, mean both particle size of 5μm, were purchased from Derivata Ind.Com. These powder were manually mixed to perform the desired stoichiometry. The theoretical density of this hardmetal is 14.7g/cm^3. Mixture was divided in samples of 1g each, approximately. Samples were put into a graphite cylinder that acts as a heater (current flow during pressing) and then assembled into a calcite capsule – responsible for the gasket formation, that ensures a good high pressure distribution into the material. Sintering treatments were carried out using a special hot press (by Ryazantyashpressmash - O138B type – 2500tons) – industrial scale, commonly used for diamonds' synthesis.

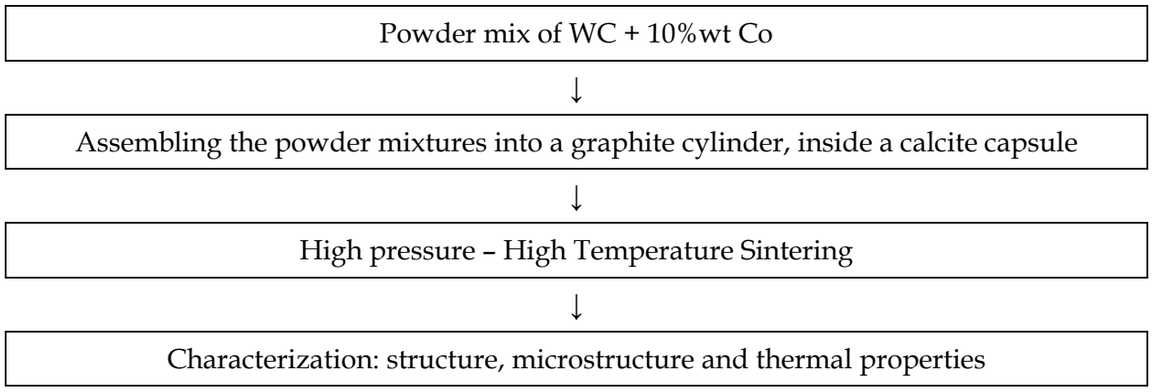

Fig. 1. Experimental flowchart for the HPHT hardmetal sintering (Rodrigues et. al, 2005)

2.2 Hardmetal processing

Hardmetals' processing is carried out by the conventional powder metallurgy – PM techniques, where the starting powders are blended, compacted in a determined part dimensions and geometry, and then sintered, whose objective is to acquire a product with controlled chemical composition, near net shape and mechanical properties (Borges *et al.*, 2008). Therefore, sintering is the most important processing step.

2.2.1 Sintering

In this step, the compacted powders are submitted to high temperature, into a furnace. During sintering several hardmetal structural changes occurs, such as densification and grain growth.

Sintering parameters like time, temperature and environment are designed for controlling the porosity level, grain size, hardness or any other desired property.

During the sintering, the Co is the binder for the WC particles, that is, the liquid phase agent. The industrial sintering temperature ranges from 1350 to 1550°C, so that Co forms an

eutectic at about 1275ºC, along with W and C – this is the so called liquid phase sintering - LPS (Allibert, 2001; Wang *et al.*, 2008).
The LPS process is divided in 3 densification stages: rearrangement, solution-precipitation and solid state sintering.
During the first stage, the compacted body behaves as a viscous solid, because the densification depends upon the liquid amount, particles' size, and solubility of the WC particles in the eutectic liquid. It forms the necks among the particles' contact points.
The solution-precipitation stage is characterized by the smaller WC particles dissolution in the liquid, which precipitates on the solid surfaces of the bigger ones. This stage enables a large densification, grains' accommodation, pores' elimination and necks' growth.
The last stage occurs when the liquid saturates. Grain growth there occurs, along with slight pore closure. It favours densification, but it is important to control the grain growth, to ensure good properties.
LPS is usually performed in furnaces with vacuum system (10^{-1} to 10^{-2} mbar), or under low pressure of gas – 0,1 MPa – for example, argon. In the last case, the goal is to reduce the porosity, and to ensure an oxygen free environment (North *et al*, 1991). It is common the use of a post-sintering process. In some cases, the use of hot isostatic pressing, at 200MPa, with the use of the same temperature and time of the previous LPS is necessary for full density.

2.2.2 High Pressure – High Temperature technology - HPHT

High pressure are those superior to 2 GPa, where some interesting changes in the materials' properties beggin to occur, like phases transformations, electrical conductivity and others (Rodrigues, 2006). That's why this technology is widely used in the production of superhard materials.
Superhard materials (SHM) synthesis such as diamond and cubic boron nitride, for example, takes place mainly in the high pressure device (HPD), using pressures ranging from 4 to 10 GPa, and temperatures of 1200 to 2000°C. The HPD are mounted inside the working space of special hydraulic presses, employing loads of 500 to 30,000 tons.
The high pressure generation is directly linked to the presses capacity and HPD construction type. The most common types of HPD are Belt, Anvil and the Multipistons. These devices are made in hardmetal – high hardness and compression resistance, with good fracture toughness, and can be processed in relatively large parts (Rodrigues, 2006). The amount of Co in this hardmetal is 4 to 6 % in weight (Bolsaitis, 1980). Table 1 shows the sintering parameters of WC-10%wtCo samples produced by HPHT.

Number of Samples	Pressure/Temperature/Time	Number of Samples	Pressure/Temperature/Time
1	5GPa/1200ºC/1min.	1	5GPa/1200ºC/2min.
1	5GPa/1300ºC/1min.	1	5GPa/1300ºC/2min.
1	5GPa/1400ºC/1min.	1	5GPa/1400ºC/2min.

Table 1. Parameters sintering of samples WC-10%wtCo sintered by HPHT

Figure 2 shows a photograph of an Anvil type HPD, already installed into the press aperture. This is the HPD used to sinter the hardmetal WC-10%wtCo of this work, and it is commonly used to produce powders of diamonds and cubic boron nitride, as well as to sinter them. The HPHT sintering process may be summarized as follows: the mixture of WC and Co powders is poured into the calcite gasket – see figure 3. Alumina and graphite discs are used for thermal insulation and direct current flux, respectively. The outer polymeric ring ensures some deformation stability for the gasket. The gasket is then mounted into de HPD. This assembly is installed into the press structure – fig. 2. The press hydraulic system generates a primary pressure P1, which raises to P2 inside the HPD – see in fig.4 the scheme of the assembly before and after pressure application. When the working pressure is reached, the electrical current system is switched on to the desired temperature inside the gasket. After the sintering time, the current is turned off, and the pressure is slowly reduced to room conditions. The HPD is removed from the press, and the sintered hardmetal sample is taken from the gasket.

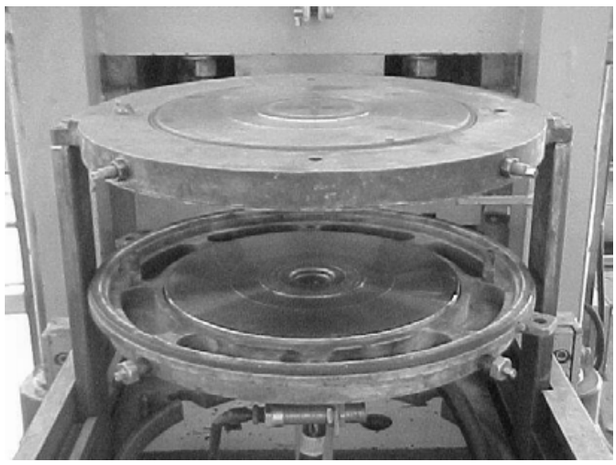

Fig. 2. Anvil type HPD

Fig. 3. Gasket with the PVC ring

Figure 4 shows, schematically, the gasket inside the HPD.

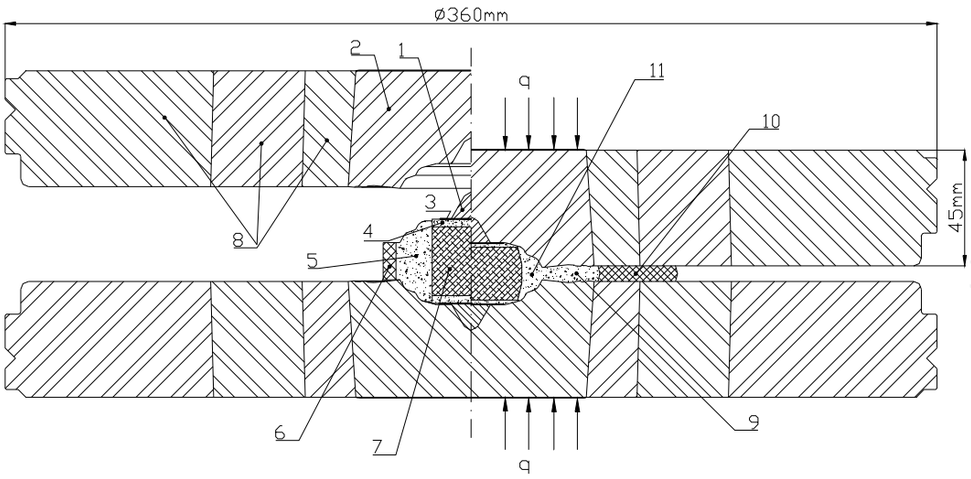

Fig. 4. Scheme of the gasket inside the HPD. (1) protective molybdenum cone; (2) anvil; (3) graphite disc; (4) alumina disc; (5) gasket prior to loading; (6) PVC ring; (7) mixed powders; (8) multi-rings; (9) gasket under loading; (10) deformed PVC ring; (11) the most deformed region of the gasket; (q) applied load

In this research, the HPHT technique was used to sinter hardmetal, aiming at the processing time reduction, and avoiding the undesirable phases formation – such as neta phases.

2.3 Photothermal science

Phothermal spectroscopy can be applied to a large number of high-sensitivity methods which measure optical and thermal properties of a sample. The basis of photothermal spectroscopy is a photo-induced change in the thermal state of the sample. The nonradiative part of light energy absorbed causes the heating of the sample. This heating is responsible for the variation of temperature and thermodynamic changes in the sample. Thus, photothermal spectroscopy is based upon measurements of temperature, pressure, or density changes that occur due to optical absorption.

Generally, photothermal spectroscopy is a more direct measurement of optical absorption than are optical transmission-based spectroscopies. Sample heating is a direct consequence of optical absorption; therefore photothermal spectroscopy signals are directly dependent on light absorption. Scattering and reflection losses do not produce photohermal signals. Consequently, photohermal spectroscopy more accurately measures optical absorption in scattering solutions, in solids and at interfaces. This characteristic makes it mostly attractive for application to surface and solid absorption analysis and studies in scattering media (Bialkowski, 1996).

The indirect nature of the measurement also results in photothermal spectroscopy being more sensitive than optical absorption measured by transmission methods. For example, photothermal effects can amplify the optical signal measured. One of the factors for this amplification is the possibility to increase the power of the light source and on the optical geometry used to excite the sample. Another feature that photohermal spectroscopy is more sensitive than transmission is that the precision of the measurements is fundamentally better than that of the direct transmission method. The high sensitivity of photothermal spectroscopy methods has led to applications for analysis of low-absorbance samples (Bialkowski, 1996).

Photohermal spectroscopy is usually performed using laser light sources. Lasers can deliver high powers or pulses energies over very narrow optical bandwidths, thereby enhancing the photothermal signals.
Here, an open photoacoustic cell (OPC) in the transmission configuration (Vargas & Miranda, 1988, 2003, Bribiesca et al., 1999) is employed to evaluate thermal diffusivity and the photothermal technique of continuous investigation illumination on the sample in a vacuum (Contreras et al., 1997) is used to measure thermal capacity density.

2.3.1 Photoacoustical investigation – measurement of thermal diffusivity

The quantity that measures the rate of heat diffusion into a material is the thermal diffusivity (α). This property depends closely on the microstructural variations, composition and the processing conditions of the sample (Raveendranath, 2006).
The OPC technique is widely used for several applications aiming at the thermal characterization of great variety of samples such as biological liquids and colloids, plant leaves, wood (López, 1996) , two layer systems (Mansanares, 1990), semiconductors (Calderon et. al., 1997), polymers (Cella et. al., 1989), clays (Alexandre et. al., 1999, Mota et al., 2008, 2009), coating materials and so on. Figure 5 shows the schematic thermal diffusivity measurement set-up.

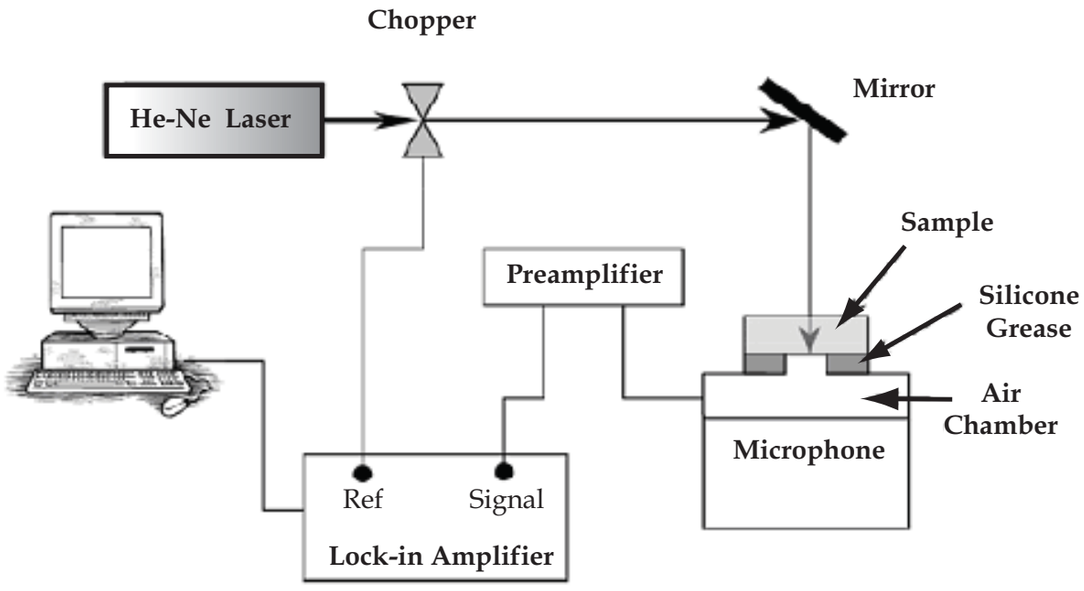

Fig. 5. Schematic measurement system of the thermal diffusivity (Yunus, 2002)

Normally, we have used a He-Ne laser (25 mW) as the excitation source. The disc sample WC-10% wt Co is mounted on the top of air chamber using vacuum grease and is illuminated on the external surface. The laser beam modulation is produced by a mechanical chopper (Stanford Research Systems SR540). The resulting PA signal is then subsequently fed into a field-effect-transistor (FET) pre-amplifier and leads directly to a "Lock-in" amplifier (Perkin Elmer Instruments mod. 5210), where it is possible to obtain the photoacoustic amplitude and the phase signal, which are recorded as a function of the

modulation frequency in an appropriate software program. The schematic cross-section of the OPC configuration is show in figure 6.

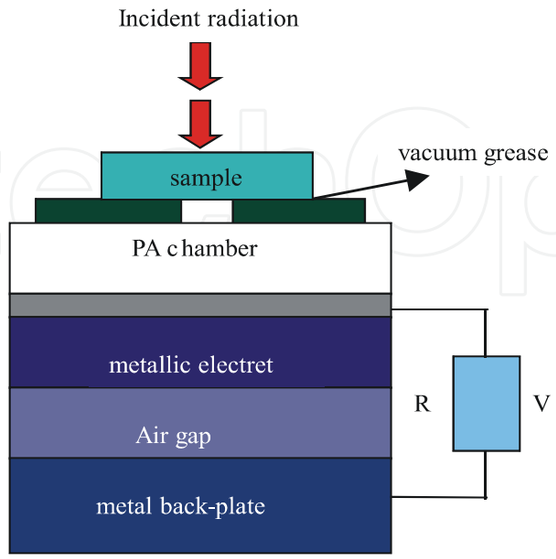

Fig. 6. Schematic design of an open photoacoustic cell (OPC)

Applying for the simple one-dimensional thermal diffusion model of Rosencwaig and Gersho (Rosencwaig & Gersho, 1976), the expression for the pressure fluctuation (δP) in the air chamber is

$$\delta P = \frac{\gamma I_0 (\alpha_g \alpha_s)^{1/2}}{2\pi l_g T_0 k_s f} \frac{e^{j(\omega t - \frac{\pi}{2})}}{senh(\sigma_s l_s)}, \tag{1}$$

where γ is the air specific heat ratio, P_0 the ambient pressure, T_0 ambient temperature, I_0 is the absorved light intensity, f is the modulation frequency, and l_i, k_i, and α_i are the length, thermal conductivity and the thermal diffusivity of the sample respectively. Here i=s subscript denotes sample and g denotes gas medium. Also $\sigma_s=(1+j)a_s$ where $a_s=(\omega/2\alpha_s)^{1/2}$ is the complex thermal diffusion coefficient of the material.
If the sample is thermally thin (i.e., $l_s a_s$ <<1), equation (2) reduces to

$$\delta P = \frac{\gamma P_0 I_0 (\alpha_g \alpha_s)^{1/2}}{(2\pi)^{3/2} l_g l_s T_0 k_s} e^{j(\omega t - 3\frac{\pi}{4})} \frac{1}{f^{3/2}} \tag{2}$$

That is, the amplitude of the PA signal decreases as $f^{1,5}$ as one increases the modulation frequency. In contrast, at high modulation frequencies, such that the sample is thermally thick (i.e. $l_s a_s$ >>1), then

$$\delta P = \frac{\gamma P_0 I_0 (\alpha_g \alpha_s)^{1/2}}{\pi l_g T_0 k_s} e^{j(\omega t - \frac{\pi}{2} l_s a_s)} \frac{e^{-l_s} \sqrt{\frac{\pi f}{\alpha_s}}}{f} \tag{3}$$

For thermally thick samples, the amplitude of the PA signal decreases exponentially with the modulation frequency as $(1/f)$ exp $(-a_s \sqrt{f})$, where $a_s = l_s \sqrt{\pi/\alpha_s}$. In this case, α is obtained from the experimental data fitting from the coefficient (a_s) in the argument of the exponential $(-a_s \sqrt{f})$.
When values of thermal diffusivity are determined from the amplitude data of the photoacoustical signal, we should pay attention to the microphone non-linear frequency response in relation to acoustical vibrations. Practically, all microphones present this irregularity. In our case, our microphone had a good linear frequency response above 20 Hz. In order to certify our set-up, a calibration measurement was performed. Figure 7 shows the dependence of the photoacoustical (PA) signal on the modulation frequency for the aluminium (Al) sample.

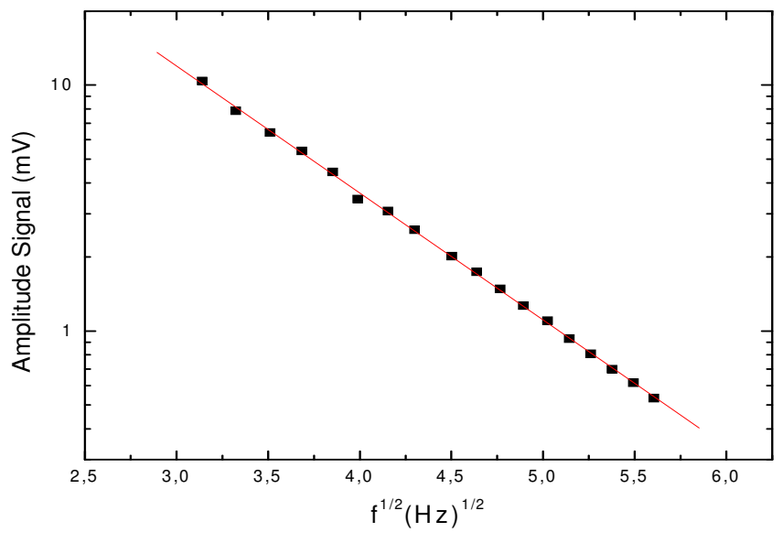

Fig. 7. Microphone output voltage as a function of the chopping frequency for the 25 μm thick Al sample. The signal behaves roughly as $f^{-1.5}$

For frequencies used to calibrate the thermal diffusivity measurement set, the signal exhibited a frequency dependency close to $f^{-1.5}$. This is the typical behaviour we would expect from the thermal diffusion model for a thermally thin sample. In fact, for a 25 μm thick Al sample and a thermal diffusivity of 93.28 x 10-6 m2/s (Almond & Patel, 1996) the characteristic frequency f_c for the transition between the thermally thin and thick regime is about 47.5 KHz.

2.4 Measurement of specific heat capacity

The product of density and specific heat, ρc, was measured using, the photothermal technique of temperature evolution induced by continuous illumination of the sample in vacuum. The surface sample is painted black and placed inside a Dewar that is subsequently vacuum-sealed. The front surface of the sample is illuminated with the He-Ne laser focused

on the sample through an optical glass window on the Dewar (figure 8). The back surface of the sample has a thin-wire T-type thermocouple. The thermocouple output is measured as in function of time by using a thermocouple monitor (model SR630 Stanford Research Systems) connected to a computer.

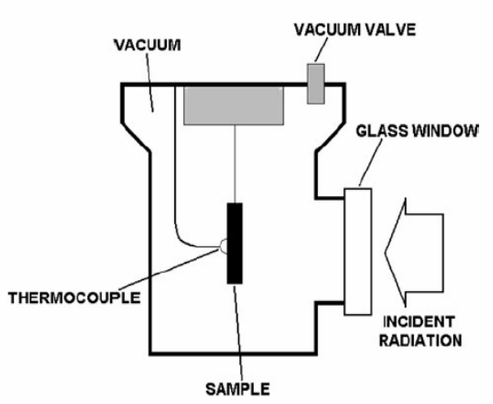

Fig. 8. Schematic measurement system of the specific thermal capacity

The temperature evolution is monitored up to reach a stationary state. Subsequently, we turn off the laser and the temperature decrease is monitored, as well. Equations 4 and 5 represent the temperature increase and temperature decrease, respectively.

$$\Delta T \uparrow = \frac{I_0}{H}(1 - e^{-t/\tau}) \tag{4}$$

$$\Delta T \downarrow = \frac{I_0}{H} e^{-t/\tau} \tag{5}$$

Finally, equations 6 and 7 present the relationship among the thermal properties. In this case, thermal diffusivity and thermal effusivity (e) are defined as in function of thermal conductivity (k) and specific thermal capacity (C), C=ρc, where c is the specific heat and ρ is the mass density.

$$k = \alpha \rho c \tag{6}$$

$$\varepsilon = \sqrt{k \rho c} \tag{7}$$

Experiments concerning with thermal diffusivity, samples thickness and specific heat capacity measurements were performed five, ten and three times to produce the deviations, respectively.

3. Results and discussion

We show in figure 9 the XRD spectra recorded for samples HPHT sintered hardmetal samples. One can observe that there is practically no difference among the samples, only WC/Co peaks are observed and the Co_3W phase in presented in all the samples. The Rietveld analysis confirmed the Co_3W phase in low intensity for the whole samples. Figure

10 shows the Rietveld analysis for 5 GPa/1200ºC/1min sample. This sample has 83,7% WC and 6.3% Co_3W.

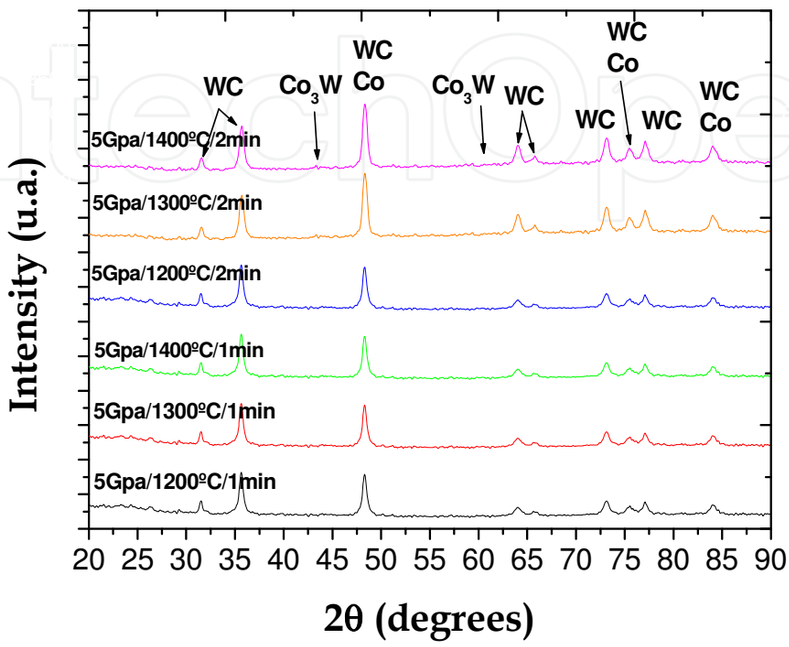

Fig. 9. X-ray diffractogram for the HPHT sintered hardmetals

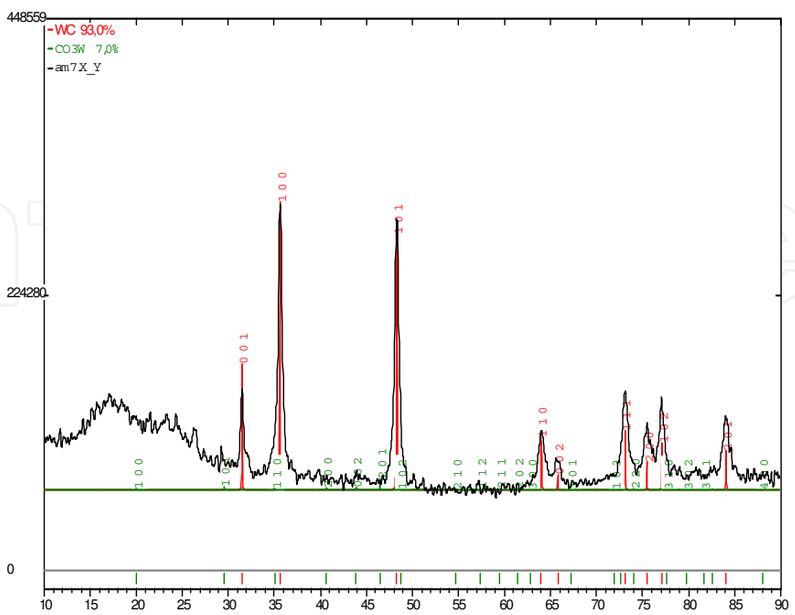

Fig. 10. Rietveld Analysis for the 5 GPa/1200ºC/1min sample

Table 2 shows the whole thermal properties reached, using our alternative method. One can see in figure 11 a typical curve for thermal diffusivity measurements for the sample subjected to 5GPa/1400ºC/2min sintering conditions. It was observed that thermal diffusivity values are; in close agreement with previous works (Miranzo et al. 2002, Lauwers et al. 2001). However, the values obtained for thermal conductivity are lower when compared with other papers (Kny & Neumann, 1985, Miranzo et al., 2002).

Samples	α (cm^2/s)	C (J/cm^3 K)	k (W/ m K)	e ($Ws^{1/2}cm^{-2}K^{-1}$)
5 GPa/1200ºC/1 min	0,340 ±0,005	1,0 ± 0,039	34,0 ± 0,040	0,58 ± 0,050
5 GPa/1200ºC/2 min	0,380 ±0,023	1,0 ± 0,042	38,0 ± 0,050	0,62 ± 0,061
5 GPa/1300ºC/1 min	0,270 ±0,046	1,0 ±0,082	27,0 ± 0,094	0,52 ± 0,107
5 GPa/1300ºC/2 min	0,250 ±0,013	0,83 ± 0,020	20,7 ± 0,020	0,41 ± 0,020
5 GPa/1400ºC/1 min	0,370 ±0,030	1,30 ± 0,080	48,1 ± 0,115	0,79 ± 0,156
5 GPa/1400ºC/2 min	0,400 ±0,006	1,0 ± 0,041	40,0 ± 0,043	0,63 ± 0,058

Table 2. Thermal properties of WC-10%wtCo sintered by HPHT

In this case, it is desirable that, within the thermal diffusivity (α), the thermal conductivity (k) also could have higher values, because the hard metal works in extreme stress situations, moreover, it is really important that the material reaches in a faster way its thermal balance, so increasing the useful life.

A possible justification for lower values is that in the conventional sintering route, due to the long time that is necessary firing process, metallic phases appear (W_3Co_3C, Co_6W_6C), which do not occur for sintering at the HPHT method. Another important factor for the low values of thermal properties is due to the not good homogeneity of the Co mixture. Although our samples present Co addition, there is phonons contribution from the phase WC heat transport. It is necessary a good crystal homogeneity for a good thermal flow, because phonons transport heat along the crystalline structure. As our HPHT samples present coalescence, porosity, phase transitions, etc, therefore phonons are easily spread out.

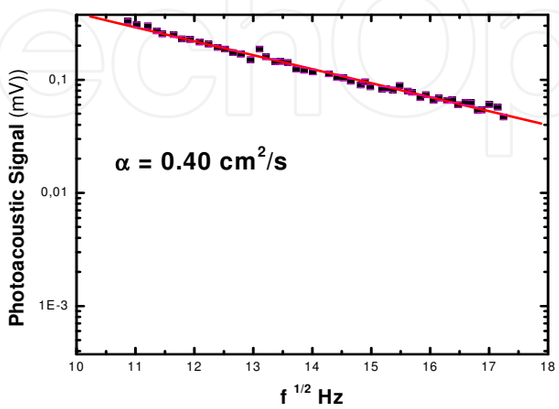

Fig. 11. Thermal diffusivity of the 5 GPa/1400ºC/2 min HPHT sintered hardmetal

The samples 5GPa/1300ºC/1min and 5GPa/1300ºC/2min presented lower values of thermal properties due to their microstructure, which do not present a good homogeneity of the WC/Co mixture, during the whole production process. Figure 9 shows the microstructure of the sintered body 5GPa/1300ºC/2min, where great cobalt lakes and a not homogeneous distribution of the Co binder are shown.
The samples sintered in 1200ºC and 1400ºC presented greater thermal property values. In figure 12 and figure 13 we can note the microstructure of 5GPa/1200ºC/1min and 5GPa/1400ºC/2min samples.

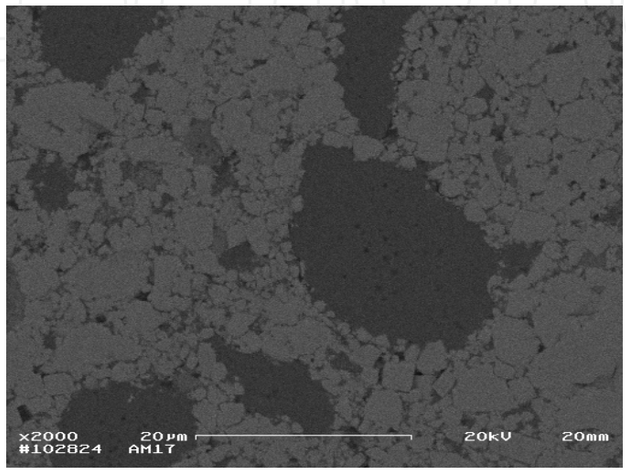

Fig. 12. Microstructure of 5GPa/1300ºC/2min sintered body

The typical hardmetal microstructure can be observed, with the grain growth of some particles of WC (white), porosity (black), and cobalt distribution (dark gray). A more homogeneous microstructure in figure 14 is observed, which presents a better cobalt distribution and presents Co lakes of the order of 5 to 15 µm, while figure 13 shows Co lakes of the order of 10 to 25 µm. The presence of a slight gray phase is observed in figure 12 (with form of spots), which are uniformly distributed. We attribute to the Co_3W phase, identified in figure 9.

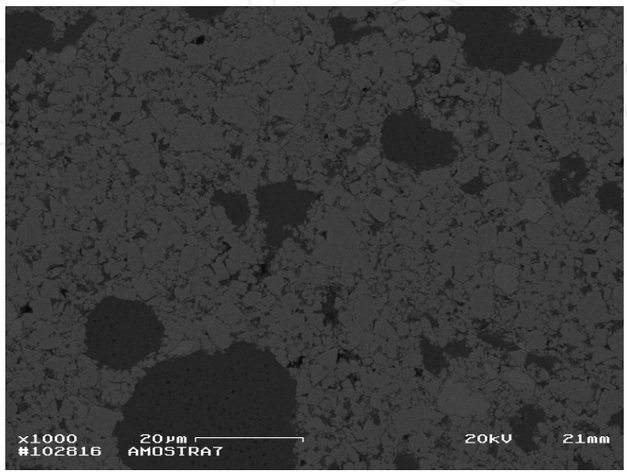

Fig. 13. Microstructure of 5 GPa/1200/1 min sintered body

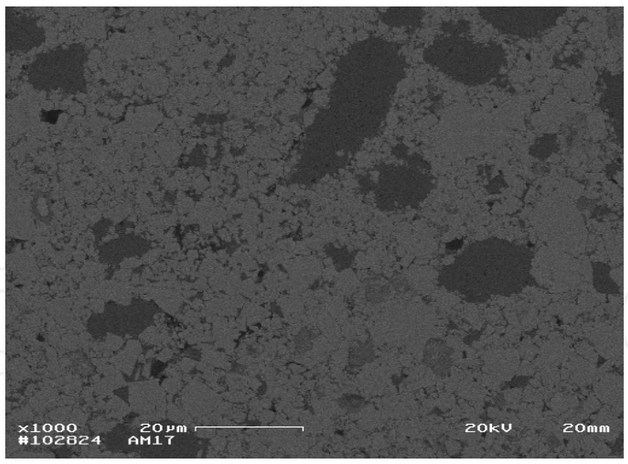

Fig. 14. Microstructure of 5 GPa/1400ºC/2 min sintered body

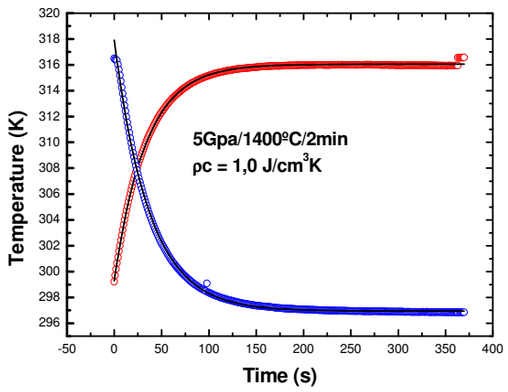

Fig. 15. Specific Heat Capacity of the 5 GPa/1400ºC/2 min HPHT sintered hardmetal

The thermal energy absorption (specific heat capacity) is lower among the samples due to a not good distribution of the metal binder. Figure 15 shows a typical curve of specific heat capacity measurements in this case 5GPa/1400ºC/2min sample.
The thermal effusivity was determined by $e = \sqrt{kC}$, which is directly influenced by the thermal conductivity and specific heat capacity. Probably, commercial hardmetals present very higher effusivity in relation to our samples. But, unfortunately, nothing can be stated, because no references were found for comparisons. We intend that these data can play an important role for this kind of material.

4. Conclusions

The goal of this exploratory work was reached. The open photoacoustic cell method is very satisfactory and readily provides thermal properties measurements for hardmetals. The metallic phases (W_3Co_3C, Co_6W_6C) occur, normally to the conventional route, while in the HPHT process there is not enough time to produce these phases. The specific heat capacity presented lower values due to the components distribution characteristics. The cobalt binder

did not disperse homogeneously in the samples, originating large Co lakes. On the other hand the thermal diffusivity values are quite realistic to the commercial hardmetals. We can conclude that is necessary more attention to the preparation sample process, mainly in the components mixture phase. The time of the WC-Co mixture should not have been sufficient for a good cobalt distribution in the sample, which harmed the results of some thermal properties. For the first time, effusivity values were determined in relation to these materials.

Essentially, for cutting and drilling tools, thermal properties play an important role in the production process. Manipulating the powders and the sintering process, it is possible to change the thermal parameters. For instance a hardmetal under study should present low thermal effusivity, that is, the outer heat flow should be blocked. Large amount of heat into the material should be avoided. However, it should present high diffusivity, high conductivity, and high thermal capacity. This way, they should expand the time-life of the tool.

5. Acknowledgments

We would like to thank UENF/FAPERJ, CNPq and CAPES for the financial support.

6. References

Alexandre, J., Saboya, F., Marques, B.C., Ribeiro, M.L.P., Salles, C., da Silva, M.G., Sthel, M.S., Auler, L.T, Vargas, H. (1999). Photoacoustic Thermal Characterization of Kaolinite Clays. *Analyst* Vol. 124, No 8, pp. 1209-1214.

Allibert, C.H. (2001). Sintering features of cemented carbides WC-Co processed from fine powders. *International Journal of Refractory Metals and Hard Materials,* Vol. 19, pp. 53-61.

Almond, D.P., Patel, P.M. (1996). *Photohermal Science and Techniques.* 1. ed.London: Chapman & Hall, 237p.

Bell, A.G. (1880). On the production and reproduction of sound by light. *American Journal of Science*, Vol .20, No 118, (October 1880) pp. 305-324.

Bialkowski, S. E. (1996), *Photothermal Spectroscopy Methods for Chemical Analysis* (1st ed.), John Wiley & Sons, Inc., New York.

Bolsaitis, P. (1980) Materials for Use in High Pressure Equipament. 1ed, Vol.1, Chapter 9 - *High Pressure Technology*. New York: Eds. Spain, I. L., Paauwe, J. 741p.

Borges, L.H.F.; Oliveira, H.C.P.; Guimarães, R.S.; Kobayashi, T.; Filgueira, M. (2008). Pressure aided Sintering of Ultrafine Powders of WC with Addition of Co. *Materials Science Forum*. Vol. 591-593, p.308-313.

Bribiesca, S., Equihua, R., Villaseñor, L. (1999). Photoacoustic Thermal Characterization of Electrical porcelains: Effect of Alumina Additions on thermal Diffusivity and Elastic Constants. *Journal of the European Ceramic Society*, Vol. 19, pp. 1979-1985.

Calderon, A., Gil, J.J.A., Gurevich, G.Y., Orea, A.C., Delgadilho, I., Vargas, H., Miranda, L.C.M. (1997). Photothermal Characterization of Electrochemical Etching Processed n-Type Porous Silicon. *Physical Review Letters.* Vol. 79, pp. 5022-5025.

Cella, N., Vargas, H., Galembeck, E., Galembeck, F., Miranda, L.C.M. (1989) Photoacoustic Monitoring of Crosslinking Reaction in Low-Density Polyethylene. *Journal Polymers Scientific Letters,* Vol 27, No 9 pp. 313-320.

Contreras. M.E., Serrato, J., Zarate, J. (1997). Photoacoustic Thermal Characterization of Lime-Partially Stabilized Zirconia. *Journal of American Ceramics Society*, Vol. 80, No 1., pp. 245-249.

Fang Z.Z. , Wang X., Taegong Ryu, Hwang K. S., Sohn, H.Y. (2009) Synthesis, sintering, and mechanical properties of nanocrystalline cemented tungsten carbide – A review. *International Journal of Refractory Metals & Hard Materials*, 27: 288-299.

Faria Jr., R.T., Filgueira, M., Esquef, I.A., Machado, F.A.L., Rodrigues, M.F., Bobrovnitchii, G.S., Vargas, H. (2005). Thermal characterization of sintered hardmetal. *Journal of Physique* IV, Vol. 125, pp. 237-239.

Faria Jr., R.T., Rodrigues, M.F., Esquef, I.A., Vargas, H., Filgueira, M. (2005). On the thermal characterization of a HPHT sintered WC–15% wt Co hardmetal alloy. *International Journal of Refractory Metals and Hard Materials*, Vol. 23, No 2, pp. 115-118.

Gille, G.; Szesny, B.; Dreyer, K.; Berg, H.; Shmidt, J.; Gestrich, T.; Leitner, G. (2002) Submicron and ultrafine Grained Hardmetals for microdrills and metal cutting inserts. *International Journal of Refractory Metals & Hard Materials*. V.20, p.3-22.

Kny, E., & Neumann, W. (1985). EinfluBgroBen auf Temperatur – und Warmeleitfahigkeit von WC-Co Hartmetallen. *High Temperatures-High Pressures*. Vol. 17, pp. 179-189.

Lauwers B., Liu W., Eeraerts W. (2002) Katholieke Universiteit Leuven, Belgium, personal communication.

López, J.A., Limon, J.M.Y., Gil, J.J.A., Vargas, H., Silva, M.D., Miranda, L.C.M. (1996). Thermal quality and structural properties of CdZnTe. *Forest Products Journal*, Vol. 46, pp. 84-89.

Mansanares, A.M., Bento, A.C., Vargas, H., Leite, N.F., Miranda, L.C.M. (1990). Photoacoustic measurement of the thermal properties of two-layer systems. *Physical Review B*, Vol. 42, No 1, (September, 1990), pp. 4477-4486.

Miranzo, P., Osendi, M.I., Garcia, E., Fernandes, A.J.S., Silva, V.A., Costa,F.M., Silva, R.F. (2002). Thermal conductivity enhancement in cutting tools by chemical vapor deposition diamond coating. *Diamond and Related Materials*, Vol 11. No 3, (March, 2002) pp. 703-707.

Mota L, Toledo R., Machado F.A.L., Holanda J.N.F., Vargas H., Faria Jr R.T. (2008). Thermal Characterisation of Red Clay from the Northern Region of Rio de Janeiro State, Brazil Using an Open Photoacoustic Cell, in Relation to Structural Changes on Firing. *Applied clay Science.* Vol 42, pp. 168-174.

Mota, L., Toledo R, Faria Jr. R. T., da Silva E. C, Vargas H., Delgadillo-Holtfort I. (2009). Thermally treated soil clays as ceramic raw materials: Characterization by X-ray diffraction, photoacoustic spectroscopy and electron spin resonance. *Applied Clay Science*, Vol 43, pp. 243-247.

North, B.; Pfouts, W.R.; Greenfield, M.S. (1991). Pressure Sinter and HIP on Cemented carbides. *Metal Powder Report*. PM Special Feature. p. 40-45.

Osipov, O., Bobrovnitchii, G., Filgueira, M. (2003). A contribution to the study of the diamond solid state sintering. *Cerâmica*, Vol. 49, No 311, pp. 151-157.

Raveendranath, K., Ravi, J., Jayalekshmi, S., Rasheed, T.M.A., Nair, K.P.R. (2006). Thermal diffusivity measurement on $LiMn_2O_4$ and its de-lithiated form (λ-MnO_2) using photoacoustic technique. *Materials Science and Engineering B*, Vol. 131, (July, 2006), pp. 210-215.

Rodrigues, M.F., Bobrovnitchii G. S., Ramalho A. M., Filgueira, M. (2005). Pressure Assisted WC-15%wtCO Sintering. *Materials Science Forum*. Vol 498-499, pp. 231-237.

Rodrigues, M.F. (2006) *Thermobaric sintering of the WC-10%pCo alloy*, MSc Dissertation. Universidade Estadual do Norte Fluminense, Campos dos Goytacazes/RJ, Brazil, 119p. In portuguese.

Rosencwaig, A., Gersho, A. (1976). Theory of the photoacoustic effect with solids. *Journal of Applied Physics,* Vol 47, No 1, (January, 1976) pp. 64-69.

Upadhyaya, G.S. (2001). Materials Science of Cemented Carbides – An Overview. *Materials and Design*. v.22, p.483-489.

Vargas, H., & Miranda, L.C.M. (1988), Photoacoustic and related Photothermal techniques *Physics Reports,* Vol. 161, pp. 43-101.

Vargas, H., & Miranda, L.C.M. (2003), Photothermal techniques applied to thermophysical properties measurements (plenary) *Rewiew of Scientific Instruments*, Vol. 74, No. 1, (January 2003) pp. 794-799.

Wang, X.; Fang, Z.Z.; Sohn, H.Y. (2008). Grain growth during the early stage of sintering of nanosized WC-Co powder. *International Journal of Refractory Metals & Hard Materials*. v 26(3), p. 232-241.

Yunus, W.M.M., Fanny, C.Y.J.; Phing, T.E.; Mohamed, S.B.; Halim, S.A. & Moskin, M.M. (2002). Thermal diffusivity measurement of Zn, Ba, V, Yand Sn doped Bi–Pb–Sr–Ca–Cu–O ceramics superconductors by photoacoustic technique. *Journal of Material Science*, Vol. 37, pp. 1055–1060.

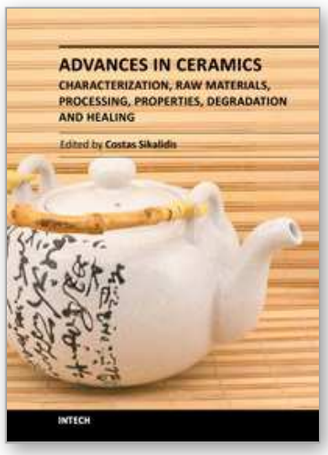

Advances in Ceramics - Characterization, Raw Materials, Processing, Properties, Degradation and Healing

Edited by Prof. Costas Sikalidis

ISBN 978-953-307-504-4
Hard cover, 370 pages
Publisher InTech
Published online 01, August, 2011
Published in print edition August, 2011

The current book consists of eighteen chapters divided into three sections. Section I includes nine topics in characterization techniques and evaluation of advanced ceramics dealing with newly developed photothermal, ultrasonic and ion spattering techniques, the neutron irradiation and the properties of ceramics, the existence of a polytypic multi-structured boron carbide, the oxygen isotope exchange between gases and nanoscale oxides and the evaluation of perovskite structures ceramics for sensors and ultrasonic applications. Section II includes six topics in raw materials, processes and mechanical and other properties of conventional and advanced ceramic materials, dealing with the evaluation of local raw materials and various types and forms of wastes for ceramics production, the effect of production parameters on ceramic properties, the evaluation of dental ceramics through application parameters and the reinforcement of ceramics by fibers. Section III, includes three topics in degradation, aging and healing of ceramic materials, dealing with the effect of granite waste addition on artificial and natural degradation bricks, the effect of aging, micro-voids, and self-healing on mechanical properties of glass ceramics and the crack-healing ability of structural ceramics.

How to reference

In order to correctly reference this scholarly work, feel free to copy and paste the following:

F. A. L. Machado, M. Filgueira, R. T. Faria Jr. and H. Vargas (2011). On the Use of Photothermal Techniques as a Tool to Characterize Ceramic-Metal Materials, Advances in Ceramics - Characterization, Raw Materials, Processing, Properties, Degradation and Healing, Prof. Costas Sikalidis (Ed.), ISBN: 978-953-307-504-4, InTech, Available from: http://www.intechopen.com/books/advances-in-ceramics-characterization-raw-materials-processing-properties-degradation-and-healing/on-the-use-of-photothermal-techniques-as-a-tool-to-characterize-ceramic-metal-materials

INTECH
open science | open minds

InTech Europe
University Campus STeP Ri
Slavka Krautzeka 83/A
51000 Rijeka, Croatia
Phone: +385 (51) 770 447
Fax: +385 (51) 686 166
www.intechopen.com

InTech China
Unit 405, Office Block, Hotel Equatorial Shanghai
No.65, Yan An Road (West), Shanghai, 200040, China
中国上海市延安西路65号上海国际贵都大饭店办公楼405单元
Phone: +86-21-62489820
Fax: +86-21-62489821

IntechOpen